ISSN 1009－3095 *Journal of Zhejiang University SCIENCE* V.3，No.5，P.501－506，Nov.－Dec.，2002
http://www.periodicals.com.cn；http://www.zju.edu.cn/English
http://www.zjupress.com；http://lib.zju.edu.cn/eindex.htm；jzu_s@mail.hz.zj.cn

Research on the orientation distribution of fibers immersed in a pipe flow*

LIN Jian-zhong(林建忠)，ZHANG Wei-feng(张卫峰)，WANG Ye-long(王叶龙)
(*Department of Mechanics，Zhejiang University，Hangzhou 310027，China*)

Received July 13，2001；revision accepted Oct.30，2001

Abstract: The computed orientation distribution of fibers immersed in laminar pipe flows showed that the longitudinal distributions are wide for small Reynolds numbers and become narrower with increasing *Re*. For low *Re* number，the axial orientation distributions are broad with almost no preferred orientations. For high *Re* number，the axial distribution becomes narrow，with sharp maxima. The mean values of the longitudinal orientation depend strongly on the *Re* number. The computed results are in qualitative agreement with relevant experimental results.

Key Words: Fiber suspension，Orientation distribution，Computation，Pipe flow
Document code: A **CLC number:** O359

INTRODUCTION

The orientation behavior of fiber immersed in fluid is an important problem in the processing of composite materials. The fiber orientation pattern is the dominant structural feature of the fiber composite，which is stiffer and stronger in the direction of greatest orientation，and weaker and more compliant in the direction of least orientation. Numerous investigations were performed during past years，regarding gravitational sedimentation and alignment of fiber in quiescent fluid. This deals with orientable fibers moving in externally imposed flows.

The spatial orientations of fiber depend on the flow velocity gradients，external forces or torque，rotational Brownian motion or local micro-turbulence. The flow velocity gradient and the fiber's rotational motion are important factors affecting the fiber orientations. The motion of fibers is influenced by forces and moments inducing them to align themselves in preferred spatial orientation. The phenomena preferred orientation of fibers was observed experimentally by Spurny et al.（1978）. Chiba et al.（1997）computed the fiber orientation in a backward-facing step channel. Ericsson et al.（1997）calculated the interaction between the flow and fiber orientation in squeeze flow. Doesburg et al.（2000）studied the preferred orientation of Au-Sn alloy plated fiber deposits. Zak et al.（2001）investigated a 3-D fiber orientation distribution in short-fiber composites by a two-section method. Burnell et al.（2001）gave the pressure-induced change in orientation order of solutes in liquid crystals. In spite of the indirect experimental evidence of the existence of preferential orientations of fibers，no quantitative information has yet been provided pertaining to these orientations and to their dependence upon the flow characteristics in a pipe. Bernstein et al.（1994）studied experimentally the orientation distribution of fibers. This paper deals with the computation of the orientation distribution of fibers moving in a pipe flow.

BACKGROUND FLOW FEILD

The background flow is pipe flow as shown in Fig.1，with velocity profile

$$u_z(r)=2u_{av}\left(1-\frac{r^2}{R^2}\right) \qquad (1)$$

where u_z is the velocity of flow in the pipe，R is the pipe radius，r is the distance to the center line，u_{av} is average velocity of flow.

* Project (No. 19925210) supported by the National Natural Science Foundation for Outstanding Youth of China

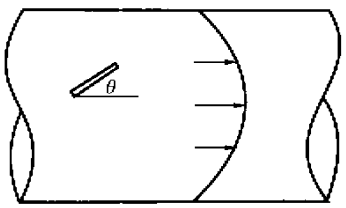

Fig. 1 Pipe flow

FIBER DYNAMICS

Basic assumption

The computations are based on the following assumptions:

1. the continuous medium hypothesis is suitable, i.e. $Kn \ll 1$.

2. fibers are non-Brownian, slender rigid cylinders (Fig. 2) in Newtonian fluid and the aspect ratio is large, $l/a \gg 1$ (l, a are the semi-length and the radius of the fiber respectively), and the end effect of cylinders is not considered.

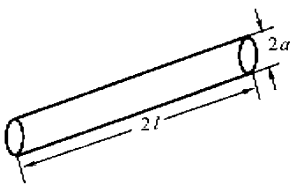

Fig. 2 Fiber

3. the length of fiber is much smaller than that of the flow field, smaller than the mesh, so that the flow around each fiber can be considered as Stokes flow.

4. the suspension is dilute, the interactions among the fibers and the lubrication effects can be neglected.

Forces and torque exerting on fibers

The fibers move under the effects of Stokes drag, added mass, Basset force and high-frequency vibration. High-frequency vibration affects the motion of the fibers to a certain degree. The complicated frequency parameter $\lambda^2 = -il^2\omega/\nu$ determines the frequency of the fiber vibration, where l is the minimum distance in the direction perpendicular to that of the fiber motion, ω is the angular frequency of the fiber vibration, and ν is the kinematic viscosity of the fluid. Comparing the viscosity relaxation time with the period of fiber vibration, we find that $|\lambda| = O(1)$. The particle velocity is given by the real part of $U_p = U_0 e^{-i\omega t}$, and the fiber displacement is U_0/ω. In fact, speed of the fiber vibration is small, namely $U_0/\omega l \ll 1$, so $Re = lU_0/\nu = |\lambda|^2(U_0/\omega l) \ll 1$.

The low- and high-frequency hydrodynamic resistance of an oscillating particle is defined by (Pozrikidis, 1988):

$$\boldsymbol{F} = \mu l Re \{\boldsymbol{R} \cdot \boldsymbol{U}_P\} \tag{2}$$

where

$$\boldsymbol{R} = \begin{cases} \boldsymbol{R}^0 + \lambda(1/6\pi)(\boldsymbol{R}^0 \cdot \boldsymbol{R}^0), & |\lambda| \ll l \\ \lambda^2 \boldsymbol{M}^A + \lambda \boldsymbol{B}^\infty, & |\lambda| \gg l \end{cases} \tag{3}$$

and $\boldsymbol{R}^0$, $\boldsymbol{M}^A$ and $\boldsymbol{B}^\infty$ signify Stokes drag, added mass, and the tensor of Basset force. For an ellipsoid with suitable aspect ratio, the results of numerical computation showed that $\boldsymbol{R}$ could be approximated very well by expansion at any frequency (Pozrikidis, 1989):

$$\boldsymbol{R} \approx \boldsymbol{R}^0 + \lambda \boldsymbol{B}^\infty + \lambda^2 \boldsymbol{M}^A + [\lambda/(\lambda+1)] \cdot [(1/6\pi)(\boldsymbol{R}^0 \cdot \boldsymbol{R}^0)) - \boldsymbol{B}^\infty] \tag{4}$$

This formula can be transformed into (3) under certain conditions. When the last parameter is small, there is extremely high accuracy. Resistance $\boldsymbol{R}$ disappears for a sphere, so the formula is precise. The Eq. (4) also can be applied to calculate the flow resistance in an unsteady flow of fibers with a proper aspect ratio. For a fiber, all the tensors have two principal values in the direction of the symmetry axis and the direction perpendicular to the symmetry axis respectively. The aspect ratio $\Phi = l/a$ is the ratio of the semi-length to radius.

In order to calculate forces on a fiber, we need to know the coefficients with a tensor form of those forces. All the tensors have two principal values, one in the direction of the symmetry axis and the other in the direction perpendicular to the symmetry axis, such as $R^0_\perp$、$R^0_{/\!/}$, $M^A_\perp$、$M^A_{/\!/}$, $B^\infty_\perp$、$B^\infty_{/\!/}$, $(R^0_{/\!/})^2/6\pi$、$(R^0_\perp)^2/6\pi$. For the above parameters, this paper adopts the experimental results (Cox, 1970) with suitable ratio. The chart form of the results given by Loewen-

berg (1993) leads to an inconvenient implementation. In this paper, the method of the least squares is used to fit each curve into a multinomial function and to obtain the coefficients of each multinomial. Then we construct a series of functions to solve for the principal values of any tensor in terms of any Φ.

Particle equation of motion

Pozrikidis (1989) deduced an expression for the force $\boldsymbol{F}$ on a vibrating fiber. $\boldsymbol{F}$ is a function of ω:

$$\boldsymbol{F} = -\mu a \{\boldsymbol{R}^0 + \boldsymbol{B}^\infty \lambda + \boldsymbol{M}\lambda^2 + (\boldsymbol{B}^0 - \boldsymbol{B}^\infty)[\lambda/(\lambda+1)]\} \cdot \boldsymbol{U} \tag{5}$$

This formula can be used to calculate the force $\boldsymbol{F}$ on a fiber. Here $\boldsymbol{R}^0$, $\boldsymbol{M}$, $\boldsymbol{B}^\infty$ represent Stokes drag, added mass force and the tensor of the Basset force respectively, $\boldsymbol{B}^0 = \boldsymbol{R}^0 \cdot \boldsymbol{R}^0/6\pi$, $\boldsymbol{U}$ is the relative velocity, and $\lambda^2 = -i\omega a^2/\nu$. The counter-transform of the formula is:

$$\boldsymbol{F} = -\mu a \left\{\boldsymbol{R}^0 \cdot \boldsymbol{U} + \frac{a}{(\nu\pi)^{1/2}}\boldsymbol{B}^\infty \int_0^t \frac{\mathrm{d}\boldsymbol{U}}{\mathrm{d}\tau} \cdot \frac{\mathrm{d}\tau}{(t-\tau)^{1/2}} + \frac{a^2}{\nu}\boldsymbol{M} \cdot \frac{\mathrm{d}\boldsymbol{U}}{\mathrm{d}t} + \frac{a}{(\nu\pi)^{1/2}}(\boldsymbol{B}^0 - \boldsymbol{B}^\infty) \cdot \int_0^t \frac{\mathrm{d}\boldsymbol{U}}{\mathrm{d}\tau} \mathrm{e}^{t-\tau}\mathrm{erfc}(\sqrt{t-\tau})\mathrm{d}\tau\right\} \tag{6}$$

The torque on a fiber is

$$L_3 = \frac{8}{3}\pi\mu\sigma l^3 (C - \dot{\theta})[1 - \sigma(\ln 2 - 1.8333)] \tag{7}$$

where $\sigma = \ln^{-1}(2\phi)$, $C = -\sin\theta\cos\theta\left(\frac{\partial u_f}{\partial x} - \frac{\partial v_f}{\partial y}\right) + \cos^2\theta \frac{\partial v_f}{\partial x} - \sin^2\theta \frac{\partial u_f}{\partial y}$, θ is the angle between fiber orientation and the pipe axis, and u_f and v_f are the components of the velocity of the flow.

Eq. (6) is divided by particle mass $m_p = \rho_p \pi l^2 a$, and then is written out with its scalar forms in the Cartesian coordinates. Eq. (7) is divided by the fiber moment of inertia round its center $J_p = \frac{m_p}{3} l^2$, and note that the flow field is steady, so there is

$$\ddot{\boldsymbol{X}} = \frac{C_1}{St}\boldsymbol{A}^{-1}\boldsymbol{R}^0\boldsymbol{A}(\boldsymbol{U}_f - \dot{\boldsymbol{X}}) + C_2\sqrt{\frac{\rho^*}{St}}\int_0^t \boldsymbol{A}^{-1}\boldsymbol{B}^\infty\boldsymbol{A}\frac{\mathrm{d}}{\mathrm{d}\tau}(-\dot{\boldsymbol{X}}) \cdot \frac{\mathrm{d}\tau}{(t-\tau)^{1/2}} - C_3\rho^*\boldsymbol{A}^{-1}\boldsymbol{M}_A\boldsymbol{A}\ddot{\boldsymbol{X}} + C_4\sqrt{\frac{\rho^*}{St}}\int_0^t \boldsymbol{A}^{-1}(\boldsymbol{B}^0 - \boldsymbol{B}^\infty)\boldsymbol{A}\frac{\mathrm{d}}{\mathrm{d}\tau}(-\dot{\boldsymbol{X}}) \cdot \mathrm{e}^{t-\tau}\mathrm{erfc}(\sqrt{t-\tau})\mathrm{d}\tau \tag{8}$$

$$\ddot{\theta} = 4\mu(C - \dot{\theta})\sigma[1 - \sigma(\ln 2 - 1.8333)]/\rho_p a^2 \tag{9}$$

here $St = \rho_p a^2 U/\delta\mu$, $\rho^* = \rho_f/\rho_p$. C_1, C_2, C_3, C_4 are four constants obtained in the method of the least squares, and $C_1 = \frac{1}{2\pi\phi}\frac{U}{\delta}$, $C_2 = \frac{1}{2\pi\sqrt{\pi\varphi}}\frac{1}{\sqrt{\delta/U}}$, $C_3 = \frac{1}{2\pi\varphi}$, $C_4 = C_2$. U and δ denote the characteristic velocity and length of the flow respectively. ρ_f is the fluid density. $\boldsymbol{U}_f$ is the velocity of the flow at the position occupied by the fiber. $\boldsymbol{X} = [x, y]^{\mathrm{T}}$ is the coordinate matrix of the fiber. The subscripts p and f denote fibers and flow respectively. $\boldsymbol{A}$ is the transformation matrix from the coordinates in the direction of the fiber axis to the Cartesian coordinates:

$$\boldsymbol{A} = \begin{bmatrix} \cos\theta & \sin\theta \\ -\sin\theta & \cos\theta \end{bmatrix}$$

From Eq. (8), we can obtain two scalar equations of x, y and their derivatives:

$$\begin{aligned} \ddot{x} &= f1 + b1 + m1 * \ddot{x} + m2 * \ddot{y} + bc1 \\ \ddot{y} &= f2 + b2 + m3 * \ddot{x} + m4 * \ddot{y} + bc2 \end{aligned} \tag{10}$$

In Eq. (10), we let

$$\frac{C_1}{St}\boldsymbol{A}^{-1}\boldsymbol{R}^0\boldsymbol{A}(\boldsymbol{U}_f - \dot{\boldsymbol{X}}) = \begin{bmatrix} f_1 \\ f_2 \end{bmatrix},$$

$$C_2\sqrt{\frac{\rho^*}{St}}\int_0^t \boldsymbol{A}^{-1}\boldsymbol{B}^\infty\boldsymbol{A}\frac{\mathrm{d}}{\mathrm{d}\tau}(-\dot{\boldsymbol{X}}) \cdot \frac{\mathrm{d}\tau}{(t-\tau)^{1/2}} = \begin{bmatrix} b_1 \\ b_2 \end{bmatrix}$$

$$C_3\rho^*\boldsymbol{A}^{-1}\boldsymbol{M}_A\boldsymbol{A} = \begin{bmatrix} m1 & m2 \\ m3 & m4 \end{bmatrix},$$

$$C_4\sqrt{\frac{\rho^*}{St}}\int_0^t \boldsymbol{A}^{-1}(\boldsymbol{B}^0 - \boldsymbol{B}^\infty)\boldsymbol{A}\frac{\mathrm{d}}{\mathrm{d}\tau} \cdot (-\dot{\boldsymbol{X}})\mathrm{e}^{t-\tau}\mathrm{erfc}(\sqrt{t-\tau})\mathrm{d}\tau = \begin{bmatrix} bc1 \\ bc2 \end{bmatrix}.$$

In the above equations, the matrix $\boldsymbol{A}$ is related to the azimuth angle. The Basset integral term and the high-frequency correction term have something to do with the accelerate course.

We cannot find an exact solution for the equations with the Basset integral term and the high-frequency, so the only way to solve them is by numerical method.

Steps of computation

1. Calculate the flow field to get the distributions of the flow velocity and $\frac{\partial u}{\partial x}$, $\frac{\partial u}{\partial y}$, $\frac{\partial v}{\partial x}$, $\frac{\partial v}{\partial y}$ in the pipe.

2. Calculate the forces on the fibers.

3. Calculate the tracks of the fibers. First, time t is divided into time points $t_i (i = 0, 1, 2, 3 \cdots)$ by unequal intervals which changes from 10^{-6} to 10^{-11} based on the requirement of precision, so the problem is transformed into solving for quantities at every point of time. Second, if the velocities, angular velocities and azimuth angles at time t_i and all the times ahead of it are calculated, we can get the acceleration at time t_i. From the acceleration, the velocity of the next time t_{i+1} can be computed approximately. Based on the velocities at t_{i+1} and all the time ahead of it, the positions of the fibers at t_{i+1} can be denoted as follows:

$$\dot{x}_{i+1} = \dot{x}_i + \ddot{x}_i \mathrm{d}t$$

$$\dot{y}_{i+1} = \dot{y}_i + \ddot{y}_i \mathrm{d}t \qquad (11)$$

$$x_{i+1} = x_i + (\dot{x}_{i-1} + \dot{x}_{i+1})\mathrm{d}t/2$$

$$y_{i+1} = y_i + (\dot{y}_{i-1} + \dot{y}_{i+1})\mathrm{d}t/2 \qquad (12)$$

4. Again, in Eq. (9), we can calculate the angular accelerations at t_i from the angular velocities and the azimuth angles at t_i, and then calculate the angular velocities and the azimuth angles at t_{i+1}:

$$\dot{\theta}_{i+1} = \dot{\theta}_i + (C - \dot{\theta}_i)L'_3 \mathrm{d}t$$

$$\theta_{i+1} = \theta_i + (\dot{\theta}_{i-1} + \dot{\theta}_{i+1})\mathrm{d}t/2 \qquad (13)$$

where $L'_3 = 4\mu\sigma[1 - \sigma(\ln 2 - 1.8333)]/\rho_p a^2$.

In the computation, when a fiber strikes the wall, the computation ends. The final steady distribution of θ is what we want to get.

RESULTS AND DISCUSSION

In order to compare the computational results and experimental ones, the same parameters of pipe flow and fiber with the experiment (Bernstein et al., 1994) were selected in the computation. The diameter of pipe was 38 mm, the mean flow velocities ranged from 0.18 to 3.7 cm/s. Fig. 3 is statistical longitudinal orientation θ for different Re number; Re number is defined based on fluid average velocity and fiber diameter. The left side gives the experimental results, the right side gives the computational ones. Abscissa is degrees of θ, ordinate r is ratio of fiber numbers which locate some region to total fiber numbers. Fig. 4 is the dependence of the mean θ upon the flow Re number. Fifty fibers were calculated in the computation. We calculated the case of seventy fibers in $Re = 51$ for trial; the disparity for different number of fibers was not evident. Because it took long time to track a fiber, we selected fifty as the number of calculated fibers.

1. Computational and experimental results were in accord qualitatively.

2. The distributions of the longitudinal orientations were asymmetric, with at least one prominent maximum observed in the range from 0° to 30°. Sometimes, an additional lower maximum could be observed at larger θ-angles. The reason was that when fibers had orientations near 0° and 90°, the torque exerted on a fiber was the least.

3. For $Re = 51$, the distributions were broad, the mode of the maxima was comparable to the neighboring modes; the longitudinal orientation distributions were broad, with almost no preferred orientations. The mode became larger at low θ values at $Re = 110$. For Re number lying between 504 and 1584, the distributions parameters were localized around θ values smaller than 30°. Therefore, the range of the mode locations depends on the flow Re number. At low Re numbers all fiber orientations seemed equally probable. With increasing Re number, the fibers' alignment with the flow direction became more obvious. This phenomenon can be explained by the fact that fiber orientation depends on the force and torque, which are related to the fluid velocity and velocity gradient. At high Re numbers, velocity and velocity gradient are higher, then the torque on a fiber which has no preferential orientation near the 0° is larger based on Eqs. (6) and (7).

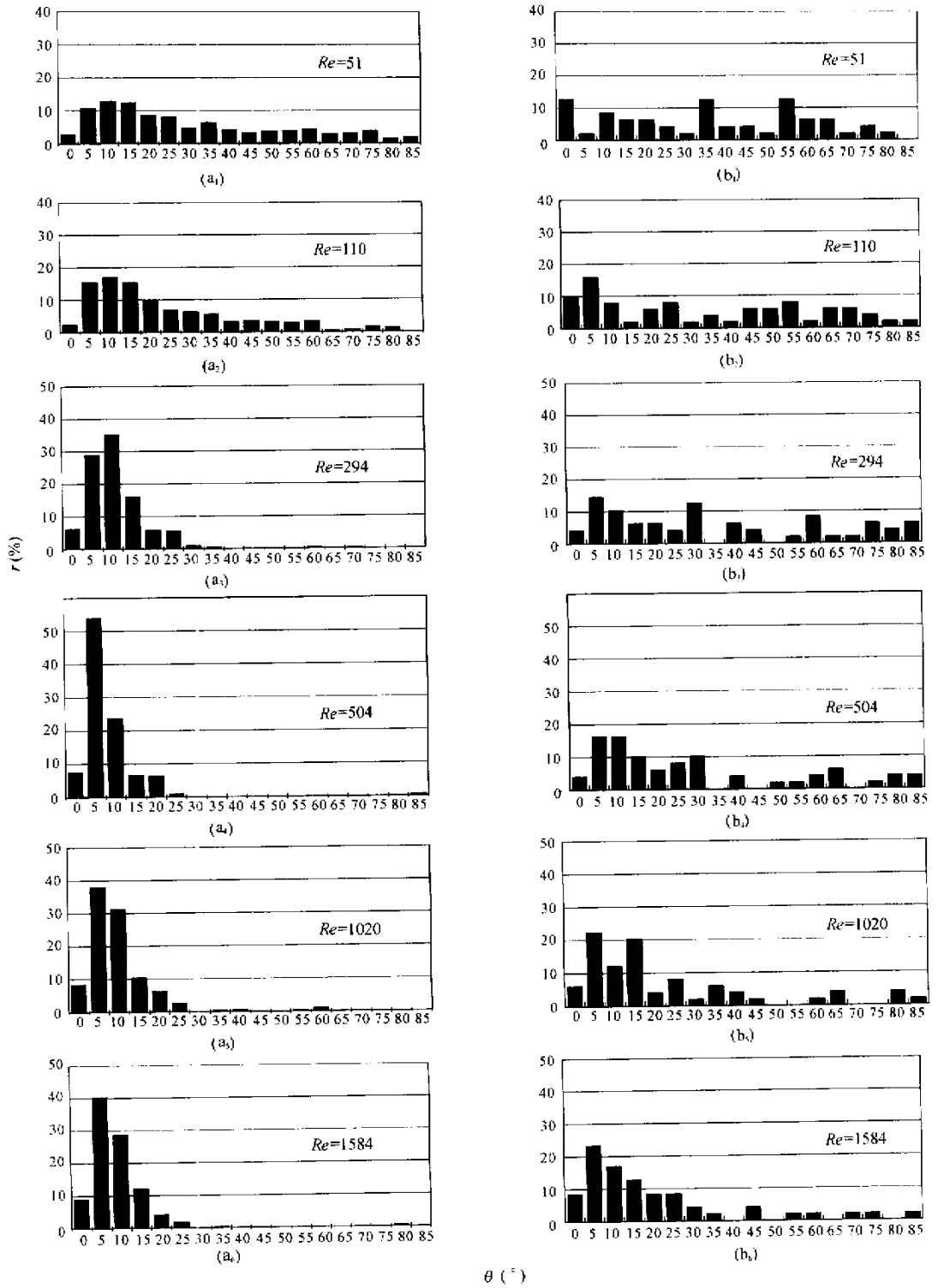

Fig. 3 The distribution of longitudinal orientation θ for different *Re* number

(a_1), (a_2), (a_3), (a_4), (a_5) and (a_6) are experimental results; (b_1), (b_2), (b_3), (b_4), (b_5) and (b_6) are computational results

4. A strong dependence of the mean of the θ-angle on the *Re* number is easily observed from Fig. 4. In the pipe flow discussed in this paper, *Re* number is a parameter controlling flows, so we give the results of the effect of *Re* number on the orientations of fibers. The effect of the fiber properties on the orientations deserves to be studied in the future.

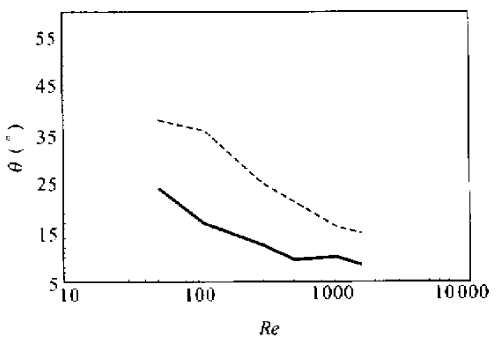

Fig. 4 The dependence of the mean θ upon the flow *Re* number

····· computational results;
—— experimental results

5. There were some differences between computational results and experimental ones. The reasons were as follows. Experimental noise influences the measured values. In the computation, the number of calculated fibers was not large enough, so because of the limit of the computer capacity, this led to error statistically.

CONCLUSIONS

The computational results, which agreed with the experimental ones qualitatively, showed the influence of *Re* number on the orientation distribution of fibers. For low *Re* number, the axial orientation distributions were broad, with almost no preferred orientations. For high *Re* number, the axial distribution became narrow, with sharp maxima. The mean values of the longitudinal orientation depended strongly on the *Re* number.

References

Bernstein, O., Shapiro, M., 1994. Direct determination of the orientation distribution function of cylindrical particles immersed in laminar and turbulent shear flows. *J. Aerosol Sci.*, **25**(1): 113 – 136.

Burnell, E. E. de lange C. A., Gaemer, S., 2001. Pressure-induced change in orientation order of solutes in liquid crystals. *Chemical physics letters.*, **337**(4): 248 – 256

Chiba, K., Nakamura, K., 1997. Numerical solution of fiber orientation in a backward-facing step channel. *Nihon Reoro. Ji. Gakk* **25**(2): 79 – 87

Cox, R. G., 1970. Long slender bodies in a viscous fluid. Part I. *J. Fluid Mech.*, **44**: 792 – 805.

Doesburg, J., Ivey, D. G., 2000. Microstructure and preferred orientation of Au-Sn alloy plated deposits. *Materials Science & Engineering.*, **78**(1): 44 – 53

Ericsson, K. A., Toll, S., Manson, J. A. E., 1997. The two-way interaction between anisotropic flow and fiber orientation in squeeze flow. *J. Rheol.*, **41**(3): 491 – 511

Loewenberg, M., 1993. Stokes resistance, added mass, and Basset force for arbitrarily oriented, finite-length cylinders. *Phys. Fluids*, A**5**(3): 725 – 734.

Pozrikidis, C., 1988. A study of linearized oscillatory flow past particles by the boundary-integral method. *J. Fluid Mech.*, **202**: 17 – 28.

Pozrikidis, C., 1989. A singularity method for unsteady linearized flow. *Phys. Fluids*, A**1**(9): 1508 – 1513.

Spurny, K. S., Gentry, J. W., Stober, W., 1978. Fundamentals of Aerosol Science (Ed. by Shaw, D. T.), Chap. 5. John Wiley, New York.

Zak, G., Park, C. B., Benhabib, B., 2001. Estimation of three-dimensional fiber-orientation distribution in short-fiber composites by a two-section method. *Journal of composite materials*, **35**(4): 316 – 330